

Effect of surface macroroughness on the microstructure and sliding wear properties of $\text{Al}_2\text{O}_3 + 13 \text{ wt.}\% \text{TiO}_2$ thick coatings

Sara I. Zesati-Belmontes^{a,b}, Enrique A. López-Baltazar^{b,*}, José J. Ruiz-Mondragón^c, Haideé Ruiz-Luna^{b,d}, Francisco Alvarado-Hernández^b, Víctor H. Baltazar-Hernández^b

^a CIATEQ, Manufactura Avanzada Sede Aguascalientes, Aguascalientes 20358, México

^b Materials Science and Engineering Program, Universidad Autónoma de Zacatecas, Zacatecas 98000, México

^c Corporación Mexicana de Investigación en Materiales SA de CV, Coahuila 25290, México

^d CONACYT - Universidad Autónoma de Zacatecas, Zacatecas 98000, México

(*Corresponding author: ealopezb@uaz.edu.mx)

Submitted: 30 August 2021; Accepted: 30 November 2022; Available On-line: 27 December 2022

ABSTRACT: Two macro-roughness patterns namely spiral grooving and diamond knurling were performed on an AISI/SAE 1045 cylindrical steel bar. $\text{Al}_2\text{O}_3 + 13 \text{ wt.}\% \text{TiO}_2$ powder was deposited by utilizing a multi-pass torch. Microstructure, microhardness and wear resistance were analyzed. The presence of both $\gamma\text{-Al}_2\text{O}_3$ and $\alpha\text{-Al}_2\text{O}_3$ throughout the coating was promoted by partially melted and un-melted particles; however, the formation of interlayers of hard $\alpha\text{-Al}_2\text{O}_3$ was influenced by the re-heating during the multi-pass torch causing transformation from $\gamma\text{-Al}_2\text{O}_3 \rightarrow \alpha\text{-Al}_2\text{O}_3$. Knurling pattern specimens contained less defects owe to a suitable splat accommodation thus strengthening the inter-splat anchorage. The improved sliding wear resistance was influenced by both the combination of $\gamma\text{-Al}_2\text{O}_3$ (toughness) and $\alpha\text{-Al}_2\text{O}_3$ (hardness) phases and, predominantly by the reduced porosity and micro-cracks in specimens with the knurling pattern.

KEYWORDS: $\text{Al}_2\text{O}_3 + 13 \text{ wt.}\% \text{TiO}_2$ coatings; Macroroughness; Sliding wear; Thermal spraying; Thick coating

Citation/Citar como: Zesati-Belmontes, S.I.; López-Baltazar, E.A.; Ruiz-Mondragón, J.J.; Ruiz-Luna, H.; Alvarado-Hernández, F.; Baltazar-Hernández, V.H. (2022). "Effect of surface macroroughness on the microstructure and sliding wear properties of $\text{Al}_2\text{O}_3 + 13 \text{ wt.}\% \text{TiO}_2$ thick coatings". *Rev. Metal.* 58(4): e232. <https://doi.org/10.3989/revmetalm.232>

RESUMEN: Efecto de la macro-rugosidad superficial sobre la microestructura y las propiedades de desgaste por deslizamiento de recubrimientos gruesos de $\text{Al}_2\text{O}_3 + 13 \%$ en peso de TiO_2 . Se realizaron dos patrones de macro-rugosidad, a saber, ranurado en espiral y moleteado de diamante, en una barra cilíndrica del acero AISI/SAE 1045. Se depositó $\text{Al}_2\text{O}_3 + 13\%$ en peso de polvo de TiO_2 utilizando un soplete en varias pasadas. Se analizó la microestructura, la microdureza y la resistencia al desgaste. La presencia tanto de $\gamma\text{-Al}_2\text{O}_3$ como de $\alpha\text{-Al}_2\text{O}_3$ en todo el recubrimiento fue promovida por partículas parcialmente fundidas y sin fundir; sin embargo, la formación de capas intermedias de $\alpha\text{-Al}_2\text{O}_3$ duro estuvo influenciada por el recalentamiento con el soplete en pasadas múltiples que provocó la transformación de $\gamma\text{-Al}_2\text{O}_3 \rightarrow \alpha\text{-Al}_2\text{O}_3$. Los especímenes con patrón de moleteado resultaron contener menos defectos debido a una acomodación adecuada de las gotas.

Copyright: © 2022 CSIC. This is an open-access article distributed under the terms of the Creative Commons Attribution 4.0 International (CC BY 4.0) License.

lo que fortaleció el anclaje entre las gotas. La mejora de la resistencia al desgaste por deslizamiento estuvo influenciada por la combinación de las fases γ -Al₂O₃ (tenacidad) y α -Al₂O₃ (dureza) y, predominantemente, por la reducción de la porosidad y las microfisuras en las probetas con patrón moleteado.

PALABRAS CLAVE: Desgaste por deslizamiento; Macro-rugosidad; Proyección térmica; Recubrimientos Al₂O₃ + 13 % en peso de TiO₂; Recubrimiento grueso

ORCID ID: Sara I. Zesati-Belmontes (<https://orcid.org/0000-0002-6226-2108>); Enrique A. López-Baltazar (<https://orcid.org/0000-0001-9792-7141>); Francisco Alvarado-Hernández (<https://orcid.org/0000-0002-8344-6379>); Víctor H. Baltazar-Hernández (<https://orcid.org/0000-0001-8629-9936>); Haideé Ruiz-Luna (<https://orcid.org/0000-0002-2799-8486>); José J. Ruiz-Mondragón (<https://orcid.org/0000-0003-1925-8610>)

1. INTRODUCTION

Alumina (Al₂O₃) is a commercially available ceramic widely employed in industry to overcome wear and corrosion issues; coatings developed with Al₂O₃ offer a reasonable cost alternative to surface protection. In particular, Al₂O₃ + 13 wt.-% TiO₂ alloy coatings provide acceptable sliding, abrasion and erosion wear resistance owe to a combination of high hardness and reliable toughness. The addition of TiO₂ has several advantages; for instance, the melting temperature and hardness decrease as the content of TiO₂ increases; on the contrary, the toughness increase by increasing TiO₂ content, thus improving the overall wear properties of the coatings (Wang *et al.*, 2000; Habib *et al.*, 2006; Yilmaz, *et al.*, 2007; Di Girolamo *et al.*, 2014; Matikainen *et al.*, 2014; Ghazali *et al.*, 2016).

Flame thermal spraying is a cost-effective method for protecting or refurbishing components and structures because: a) it is easy to handle and quite adaptable to manufacturing processing and the automation is not needed; b) it is portable and easy to use as the operators do not require high-level of training; c) it produces lower dust and fume levels and the security equipment for operation is not highly sophisticated as compared to other thermal spraying processes; d) it is easy to coat parts or components with complex geometries due to the possibility of utilizing manual operation; e) it inputs lower distortion to substrate due low heat transfer; and f) it is suitable to be employed in environments which are less demanding. Flame spraying is often used to repair and/or protect industrial components subjected to sliding wear such as shafts, bearings, gears, or similar surfaces, by utilizing an ample variety of materials as feedstock (Oerlikon Metco, 1945; Romero, 1990; ASTM Committee, 1994; Davis, 2004).

Adhesion is one of the most important characteristic of thermally sprayed coatings that strongly influence on the wear performance; thus, the surface roughness of the substrate is of critical importance since this guarantees suitable mechanical anchorage or mechanical interlocking (Davis, 2004; Wang *et al.*, 2005). In low velocity thermal spraying processes i.e. flame spraying and/or in processes where exist un-melted particles; mechanical interlocking of the splat within the substrate irregularities is the principal bonding mechanism influencing on the adhesion strength in coatings (Pare-

des *et al.*, 2006). Roughening is a critical step in preparing the surface before the coating application as the former ensures proper adhesion. Therefore, in order to obtain adequate roughening; the substrate surface must be correctly prepared and various common methods can be utilized viz. rough threading (used for cylindrical surfaces), grit blasting, and/or a combination of the previously mentioned (ASTM Committee, 1994).

Thick coatings are found in various situations such as: built-up or reconditioning of machine parts, repairmen of components, thermal barrier, wear protection, corrosion protection, among others. Nevertheless, processing of thick coatings is not an easy task and several problems must be faced: i.e. weak mechanical anchoring (poor adhesion) (Berndt and McPherson, 1979), presence of edge delamination failure (Bordeaux *et al.*, 1991), increasing of residual stresses with thickness (Tucker, 1974), generation of microcracks (Steffens *et al.*, 1999).

Macro-roughening (an easier to handle technique, faster, and economical) is commonly applied for restoring greater dimensions (thick coatings) in damaged surfaces. Macro-roughening can be performed on shafts through a lathe machine operation by cutting a narrow, low-pitch, shallow groove or thread in the surface (Romero, 1990). It is worth mentioning that macro-roughening is an effective technique for residual stress reduction by inducing folds in the coatings thus promoting low shrinkage. In addition, macro-roughening can prevent shear or edge delamination, and further reduce cracking and/or spalling in coatings (Tucker, 1974; James, 1984; Bordeaux *et al.*, 1992; Matějčíček *et al.*, 2007; Hollis *et al.*, 2007). However, there is a lack of information in the literature relating the cylindrical surface macro-roughness viz. knurling and grooving, to the resultant microstructure and sliding wear performance upon flame spraying of thick coatings.

This study aims at evaluating the effect of the cylindrical surface macro-roughness on the overall microstructure and sliding wear behaviour of Al₂O₃ + 13 wt.-% TiO₂ thick coatings deposited on a AISI/S&A E 1045 steel bar, using two different machining methods as anchorage viz. spiral grooving and knurling pattern.

2. MATERIALS AND METHODS

A commercial (Oerlikon MetcoTM), agglomerated and sintered Al₂O₃ + 13 wt.-% TiO₂ powder alloy with

a particle size distribution of $-45+15 \mu\text{m}$ ($d_{50}=30.9 \mu\text{m}$) was used as feedstock in this work (Fig. 1). An Oerlikon Metco™ Ni-5Mo-5.5Al powder alloy with size distribution of $-90+45 \mu\text{m}$ ($d_{50}=59.6 \mu\text{m}$) was additionally employed as bond-coat in order to improve the adhesion of alumina to the substrate.

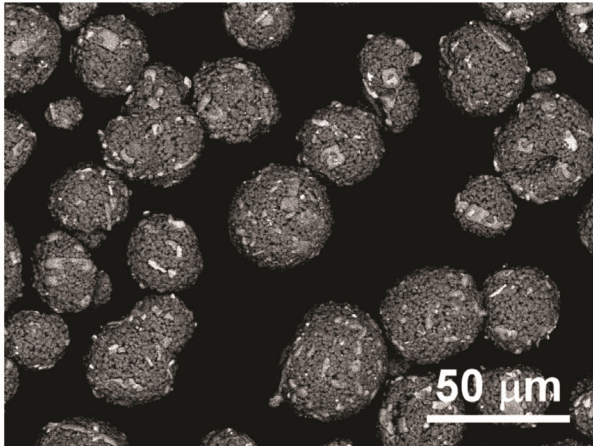


FIGURE 1. Morphology of the agglomerated and sintered $\text{Al}_2\text{O}_3 + 13 \text{ wt.}\% \text{ TiO}_2$ powder.

An AISI/SAE 1045 cylindrical steel bar with diameter of 31.75 mm and 256 $\text{HV}_{0.5}$ in hardness was used as substrate. A drilled hole (15 mm in diameter) was performed in the center of the cylinder; afterwards, the steel bar was cross-sectioned with the purpose of forming a ring specimen of 5 mm in thickness.

Four different macro-roughened surfaces were prepared at the outer surface of the ring specimens: two diamond pattern knurling (DKA and DKB), and two spiral pattern grooving (SGA and SGB). Geometry and dimensions of the surface profile for both DK and SG patterns are indicated in the schematic of Fig. 2.

Before the coating deposition, all specimens were properly cleaned in an ultrasonic bath. The coating deposition was conducted towards the outer surface of the ring specimen, as it is shown in Fig. 3a, by using a CastoDyn DS8000™ thermal spray gun. Just after eight preliminary trials; suitable deposition parameters for $\text{Al}_2\text{O}_3 + 13 \text{ wt.}\% \text{ TiO}_2$ powders were obtained as it is listed in Table 1, the deposition parameters were constant for all conditions. Multi-pass torch (6 passes in total) was performed to obtain thick (1000-1200 μm) $\text{Al}_2\text{O}_3 + 13 \text{ wt.}\% \text{ TiO}_2$ coatings.

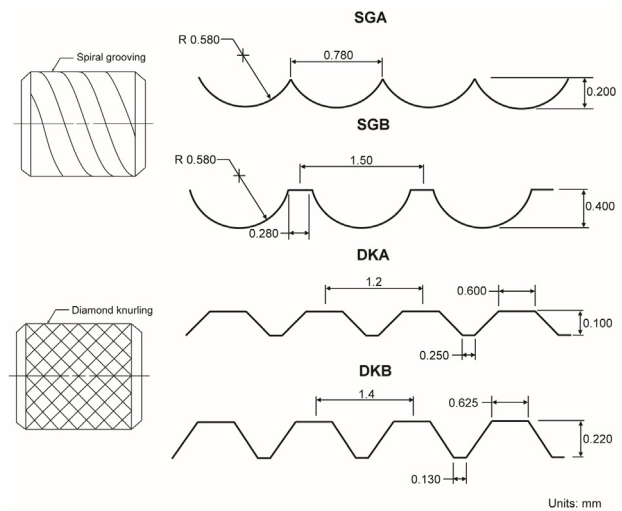


FIGURE 2. Drawing showing the surface patterns and dimension profile for: the spiral grooving (SG) and the diamond knurling (DK).

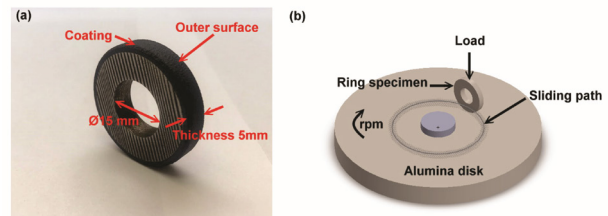


FIGURE 3. (a) Ring specimen configuration, (b) Sliding wear testing setup.

The coated specimens were sectioned in the transverse direction. After performing the usual metallographic procedures all micrographs were taken in a Tescan Mira3™ scanning electron microscope. By following the ASTM E384 (2017) hardness standard and employing a Shimadzu tester, Vickers hardness was measured with 500 g (4.905 N) of applied load and a dwell time of 15 s. Three linear paths of indentations parallel to each other with a minimum number of 8 indentations (located 200 μm apart as a minimum to each other) were obtained at the substrate and throughout the coating thickness in all specimens, it is important to declare that porosity was avoided when placing the hardness indentations. The coatings were evaluated by X-ray diffraction (XRD) using $\text{Cu-K}\alpha$ radiation on a D8Advance Bruker diffractometer by setting up a scan step of 0.002° (2θ) and a time per scan of 1 s. The stan-

TABLE 1. Flame spraying deposition parameters.

Material	Powder feeding rate (Kg/h)	Air Pressure (Bar)	Oxygen Pressure (Bar)	Acetylene Pressure (Bar)	Spraying Distance (mm)	Flame type	Nozzle diameter (mm)
$\text{Al}_2\text{O}_3 + 13 \text{ wt.}\% \text{ TiO}_2$	7.4	3.0	4.0	0.7	200	Neutral	1.25
Ni-5Mo-5.5Al	7.4	3.0	4.0	0.7	150	Neutral	2.4

standard test method ASTM E2109–01 (2021) was used for determining the area percentage porosity in the thermal sprayed coatings using image analysis.

Sliding wear testing was conducted as per the configuration illustrated in Fig. 3b. An Al_2O_3 disk with an initial roughness of $R_a=18\ \mu\text{m}$ and hardness within a range of 2110–2450 HV was utilized as counterface. Sliding wear testing was conducted by setting up a constant load of 16 N, a rotational speed of 450 rpm, and a fixed sliding distance of 1979 m. All samples were cleaned with an ultrasonic acetone bath and weighed before and after the trial in $\pm 0.01\ \text{mg}$ AUW220D Shimadzu™ precision balance with the purpose of evaluating mass loss of the specimen. Four replicas per condition were subjected to sliding wear testing at room temperature.

3. RESULTS

The corresponding cross-sectioned microstructure of the $\text{Al}_2\text{O}_3 + 13\ \text{wt.}\% \text{TiO}_2$ coatings deposited onto four different macro-roughened surfaces is shown in Fig. 4. The Ni-5Mo-5.5Al bond coat (hereafter named as “Ni bonding layer”) with an average layer thickness of $177\ \mu\text{m}$ was properly anchored to the steel substrate. The subsequent flame sprayed region is composed of various layers of $\text{Al}_2\text{O}_3 + 13\ \text{wt.}\% \text{TiO}_2$ that form the final thick coating structure.

The porosity (as pointed by black arrows) was revealed throughout the thickness of the coating in both

spiral grooving surface conditions (SGA and SGB); it is worth mentioning that higher density of porosity is located about the tip of the threads (Fig. 4a-b). Porosity is clearly correlated to the sharp tip and the slope of the groove. Due to the grooving surface is not parallel to the particles stream; there is poor adhesion along the slope of the grooves, and additionally, few particles are trapped around the sharp tip, thus promoting porosity. On the other hand, porosity is also observed upon the knurling conditions (DKA and DKB) as shown in Fig. 4c-d; however, there is a clear reduction in porosity content as compared to the SGA and SGB conditions. The absence of a sharp tips as well as the reduced slope of the grooves over the substrate actually creates an extensive active zone, leaving a larger amount of deposited particles onto the surface with reduced porosity. The porosity percentage is clearly reduced from 8.2% in spiral grooving pattern up to 3.5% upon knurling pattern due to the macro-roughness effect.

Based on the abovementioned results, the surface topography viz. macro-roughness has a clear effect on the distribution and density of porosity; for instance, the absence of sharp tips and the reduced slope in the knurling conditions, led to a reduction in porosity; an indirect evidence of acceptable adhesion conditions. Indeed, the top surface of the coating takes the original shape of the initial substrate macro-roughness, for this reason a smoother surface can be obtained when employing the knurling pattern.

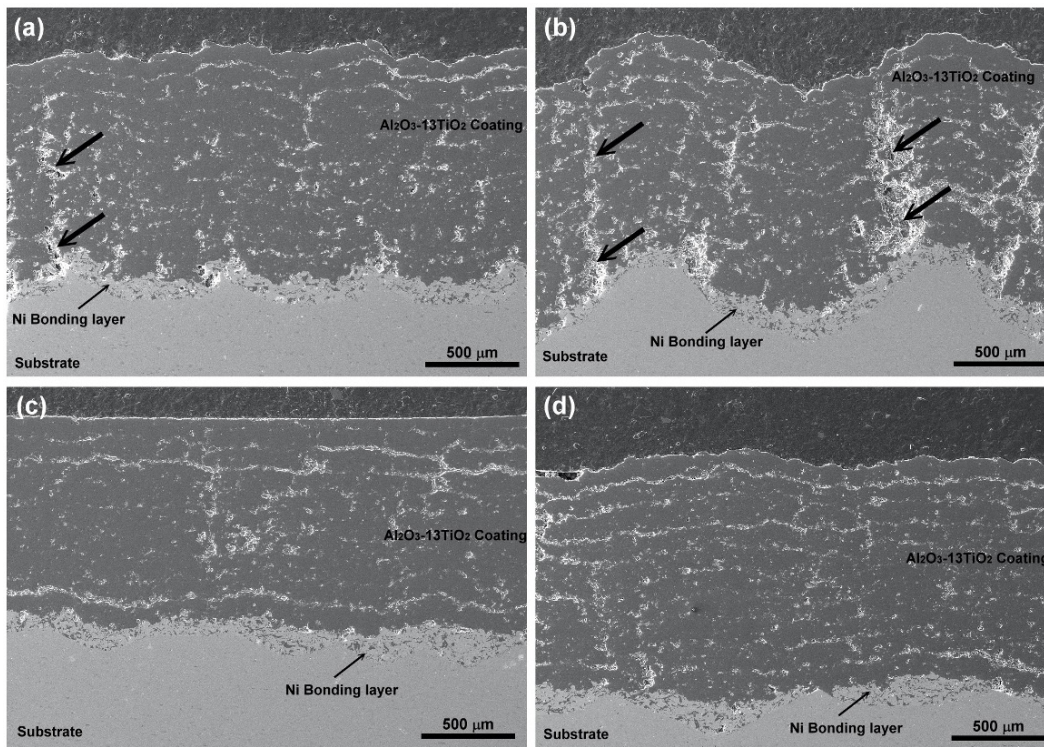


FIGURE 4. Macrostructure of the $\text{Al}_2\text{O}_3 + 13\ \text{wt.}\% \text{TiO}_2$ coatings deposited onto the grooving surface: (a) SGA, (b) SGB, and the knurling surface (c) DKA and (d) DKB.

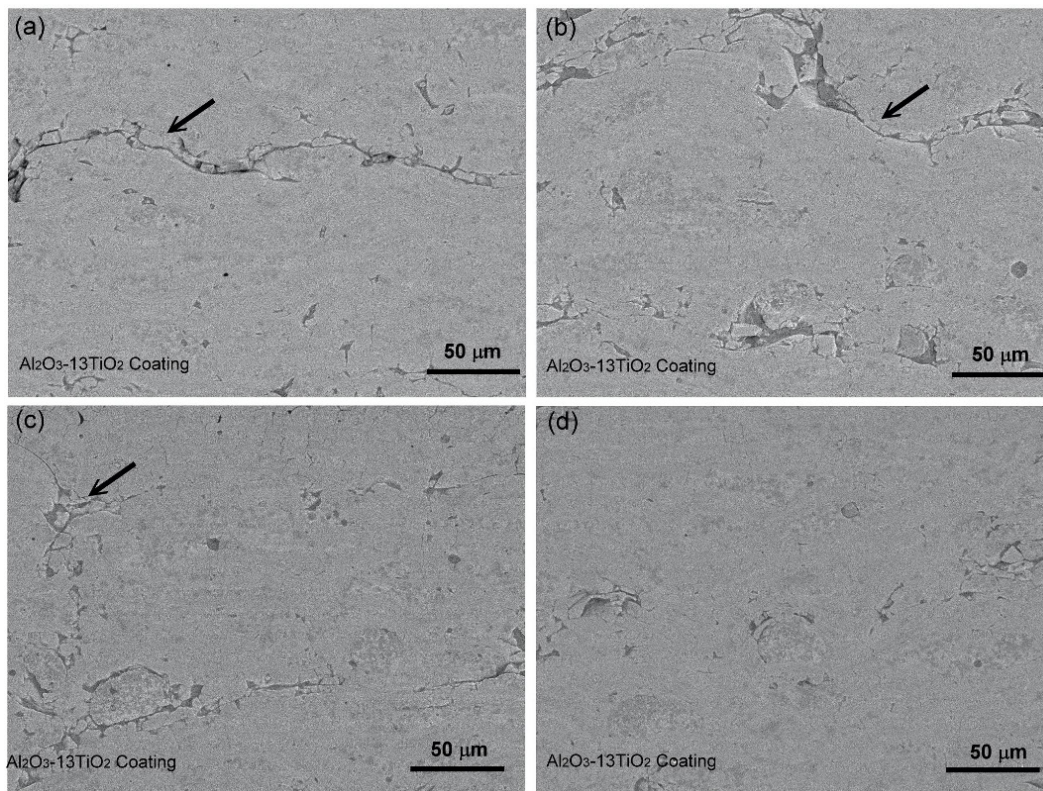


FIGURE 5. Microstructure of the $\text{Al}_2\text{O}_3 + 13 \text{ wt.}\% \text{TiO}_2$ coatings deposited onto grooving surface: (a) SGA, (b) SGB, and knurling surface (c) DKA and (d) DKB.

A lamellar structure formed by the particle impact and the subsequent flattening of splats commonly found in flame spraying processes is observed in all $\text{Al}_2\text{O}_3 + 13 \text{ wt.}\% \text{TiO}_2$ coatings (Fig. 5). A relatively dense microstructure with distinguishable microcracks is revealed; however, the extension of cracking depended on macro-roughness condition, hence, visibly dense and coarser microcracks are observed upon the SG pattern (Fig. 5a-b); whereas, a reduced fraction of thinner microcracks are revealed upon the DK condition as shown in Fig. 5c-d. It is clear that microcracks are minimized upon the pattern knurling DKA and DKB.

Microcracks are the product of the shrinkage due to rapid solidification of the deposited particles on the surface. Both spiral grooving conditions resulted in coarser and larger microcracks due to abrupt surface geometry changes (i.e. sharp tips, with high slope within the groove shape), thus causing distortion during the splat disposition affecting the shrinkage pattern, and hence, the inter-splat adhesion. On the other hand, a properly defined pattern such as knurling, ensures uniform surface geometry changes, free of sharp-tips, and reduced slope, the splats are properly trapped to the substrate with smooth geometry changes, having an effective deposition, thus facilitating the stacking (coating build up), and promoting good inter-splat adhesion. Therefore, it is again inferred that the surface topography greatly affects the characteristics of microcracks present in the coatings. Predominantly melted regions

are encounter in all coatings; however, partially melted and/or un-melted round particles are also revealed.

XRD analysis of the feedstock powder provided in Fig. 6a, shows the presence of stable $\alpha\text{-Al}_2\text{O}_3$ and TiO_2 (rutile) phases along with a reduced fraction of Al_2TiO_5 , which can be ascribed to the sintering reaction of $\text{Al}_2\text{O}_3 + 13 \text{ wt.}\% \text{TiO}_2$ powder mixture during the manufacturing process of the powder.

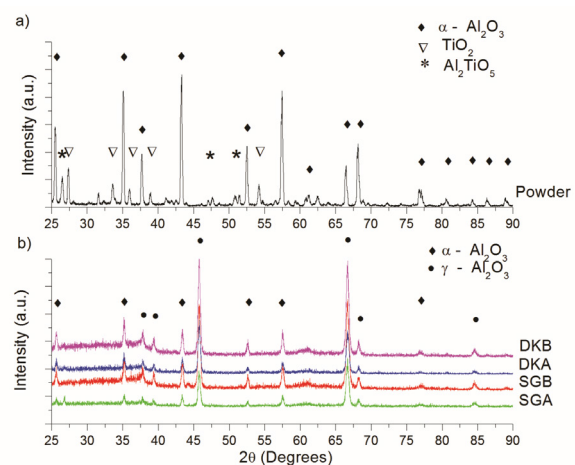


FIGURE 6. XRD diffraction patterns of $\text{Al}_2\text{O}_3 + 13 \text{ wt.}\% \text{TiO}_2$ powder and sprayed coatings DKB, DKA, SGB and SGA pattern.

No differences in terms of phase transformation were found among SGA, SGB, DKA and DKB conditions as shown in Fig. 6b. Transformation from α -Al₂O₃ phase to the metastable γ -Al₂O₃ phase during flame spraying processing resulted in all specimens as it is seen in Fig. 6b, not evidence neither of TiO₂ nor Al₂TiO₅ was recorded. The transformation from α -Al₂O₃ phase to γ -Al₂O₃ phase during solidification is attributed to its lower critical free energy for nucleation; on this basis, γ -Al₂O₃ would be nucleated rather than α -Al₂O₃ at low temperatures (McPherson, 1973; R. McPherson, 1980; Fervel *et al.*, 1999; Normand *et al.*, 2000; Yilmaz *et al.*, 2007; Di Girolamo *et al.*, 2014).

Interestingly, a semi-quantification analysis made to the multilayered coating (obtained with more than one torch pass) resulted in an average fraction of approximately 25% of α -Al₂O₃ and 75% of γ -Al₂O₃. In further analysis, XRD was executed in a single layer coating (obtained with only one torch pass) thus resulting in 5 to 10% content of α -Al₂O₃; hence, the presence of α -Al₂O₃ is correlated to the partially melted and/or the un-melted particles in single-layered coatings (Normand *et al.*, 2000; Lou *et al.*, 2003; Yilmaz *et al.*, 2007; Di Girolamo, *et al.*, 2014; Yang *et al.*, 2015). However, the remained fraction of α -Al₂O₃ phase in the multilayered specimens, is absolutely related to re-transformation of γ -Al₂O₃ \rightarrow α -Al₂O₃ during the multi-pass torch spray processing (reheating). For instance, during the deposition process; the melted particles resulted in full transformation from α -Al₂O₃ to γ -Al₂O₃ phase; nevertheless, with the subsequent passing of the torch on the already deposited layer, a localized heat treatment is developed with enough temperature for causing γ -Al₂O₃ \rightarrow α -Al₂O₃ reversed transformation. It is well known that transformation

from γ -Al₂O₃ to α -Al₂O₃ phase is possible when heating the substrate approximately about 1100 °C (McPherson, 1980; Di Girolamo, *et al.*, 2014). It is important to mention that approximately 15 to 20% of the preliminary layer is re-transformed to α -Al₂O₃ due to the fact that the maximum temperature for transformation penetrates few microns within the previous layer. The subsequent torch passes created a layering which combines the presence of thinner α -Al₂O₃ phase and thicker γ -Al₂O₃ phase layers as schematically depicted in Fig. 7a. It is worth mentioning that spraying parameters (nozzle, flame type, spraying distance, etc.) were constant for all specimens; then it is deduced that the surface geometry has no effect on the phase transformation of the coatings as no differences are observed according to XRD.

Figure 7b, shows the micro-hardness profile taken from the substrate throughout the coating thickness. A schematic depicting the paths of hardness indentations on the various regions viz. substrate and the Al₂O₃ layering is provided in Fig. 7a. The hardness of the substrate averaged 256 HV_{0.5}, whereas the mean value hardness of the alumina layering was 972 HV_{0.5}. A clear fluctuation of the hardness values is observed along the coating in all specimens which is markedly related to the distinct α - and γ -Al₂O₃ layers throughout the coating. Therefore, as some indentations lay into α -Al₂O₃ and others into γ -Al₂O₃ along the distance from the substrate/coating line over the coating; the higher hardness values are correlated to α -Al₂O₃ because of its highest hardness as compared with γ -Al₂O₃ phase (Yilmaz, 2009; Singh *et al.*, 2011; Islak *et al.*, 2012).

Wear track of multi-layered Al₂O₃ + 13 wt.-% TiO₂ coatings are shown in Fig. 8. Scratched surfaces are revealed for all specimens. Severe wear damage is

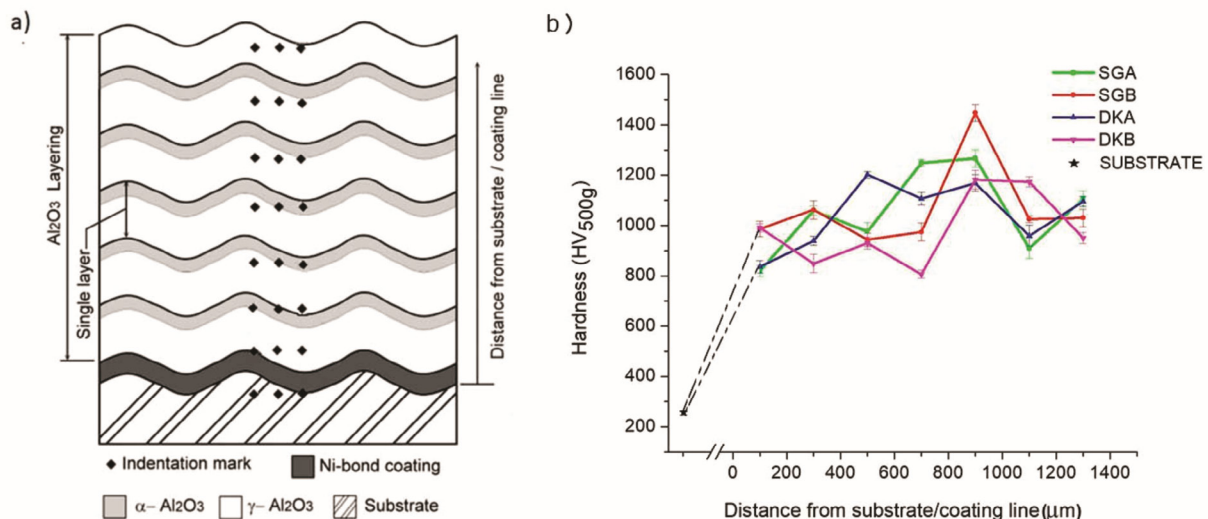


FIGURE 7. (a) Schematic diagram of the coating layers and phase transformations along the distance from the substrate, and (b) Micro-hardness profile.

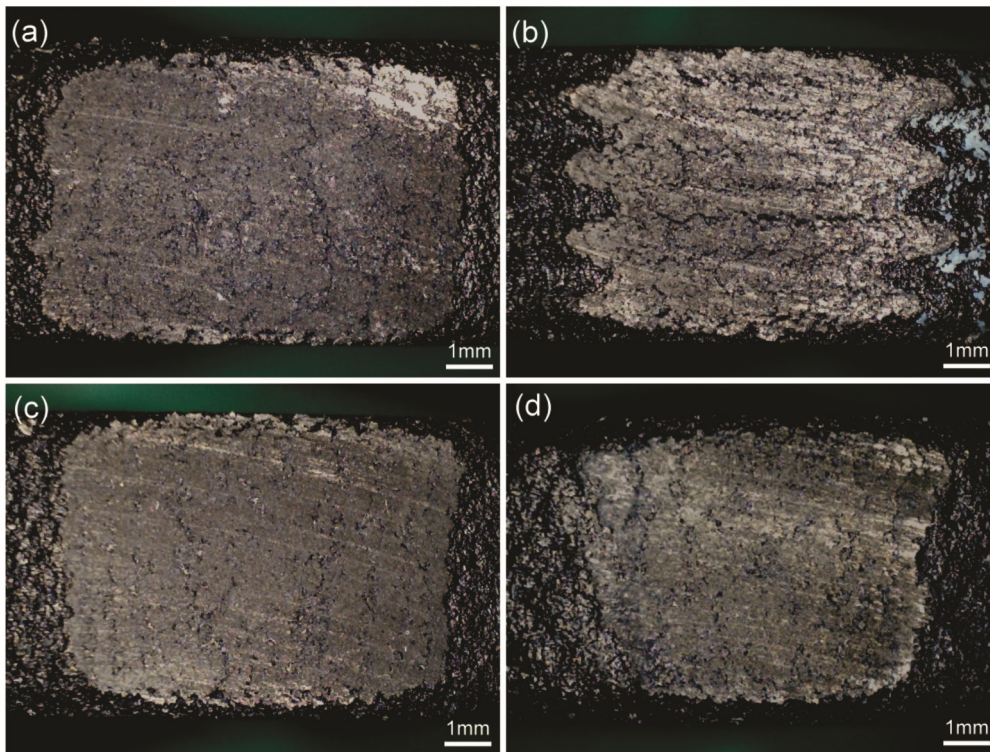


FIGURE 8. Wear track of the spiral grooving surface: (a) SGA, (b) SGB, and the knurling surface (c) DKA and (d) DKB.

clearly observed upon SGB condition followed by SGA. Coating defects (i.e. cracks) located parallel to the sliding wear track are clearly distinguishable in

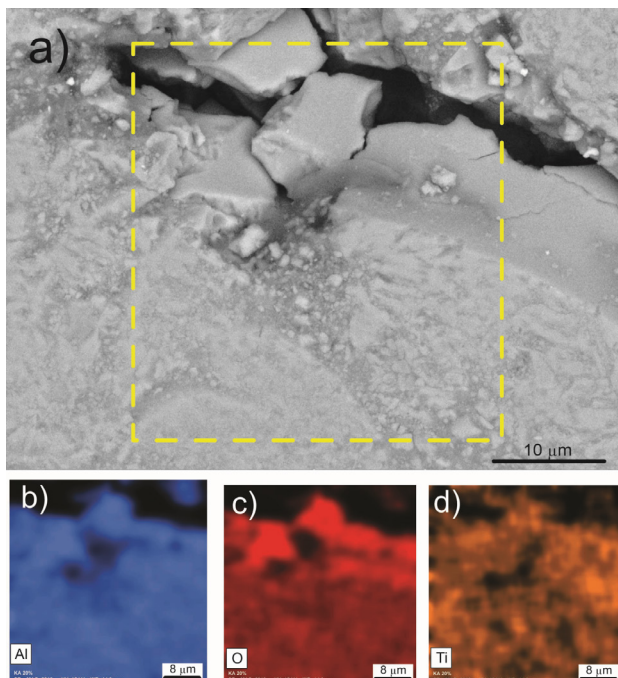


FIGURE 9. a) shows the presence of microcracks, porosity, as well as detached out particles (debris) from the coating. The yellow dashed square corresponds to the analyzed (EDS) region thus confirming the presence of (b) Al, (c) O and (d) Ti.

Fig. 8b. On the contrary, coating defects in SGA, DKA and DKB conditions are perpendicular to the wear tracks. The initial contact area between the counter disk (alumina) and the coating is minimum; in fact, the actual contact area is supported by the coating tips inherited by the substrate geometry. Once the sliding friction displacement has begun; coalescence of existing cracks as well as nucleation of new ones are generated, following this, particles are detached out from coatings (debris), it is worth mentioning that the presence of porosity and microcracks also generate splats exfoliation (as shown in the SEM micrograph in Fig. 9) (Normand *et al.*, 2000; Psyllaki *et al.*, 2001; Michalak *et al.*, 2021), which is conducted by the weak splat unions and microcracks, the above mentioned produce a progressive increment in contact area by the constant material removing from the tips. Additionally, the hard debris trapped at the inter-face between the disk and the coatings promotes the abrasion mechanism. Actually, debris is generated from both: the detached splats coming from coatings and the separated material from the counter disk. Scratching scar demonstrates an abrasion mechanism involved in the wear process.

Figure 10, shows the relationship between the wear ratio (coating mass loss/ substrate Mass loss) and porosity. It is seen that the specimens with the knurling pattern possess a higher wear resistance as compared to specimens with the spiral grooving pattern. It is clear that the wear ratio is higher when the porosity increases; for instance, SGB specimen having the larg-

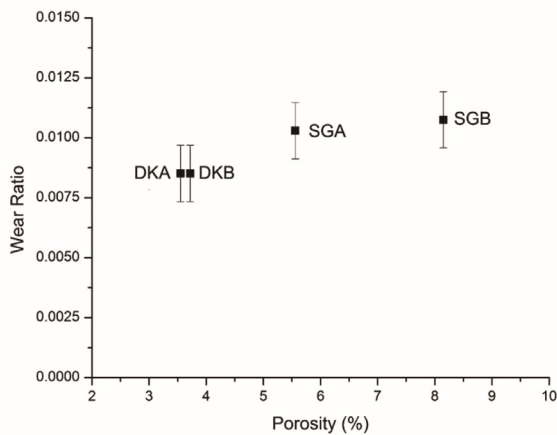


Figure 10. Relationship between the wear ratio and the porosity for the patterns SGA, SGB, DKA and DKB.

est amount of porosity and microcracks (Fig. 8b) had a higher wear ratio. Therefore, the porosity influenced on the wear resistance by weakening the splats joining; if porosity the increases, splats adhesion is logically reduced by promoting splats detachment, which clearly affects the wear resistance. Furthermore, microcracks limit splats contact, influencing on splats adhesion, and consequently on the coating toughness. If splats joint is deficient, then the toughness is reduced thus facilitating splats decohesion during wear.

4. CONCLUSIONS

- The type of cylindrical surface macro-roughness pattern had a clear effect on the distribution and density of the porosity, the absence of sharp tips and the reduced slope of the threads upon the knurling pattern led to a reduction in the porosity content. In addition, the top surface of the coating inherits the initial shape of the substrate leading to a smoother final surface when employing the knurling pattern.
- The amount and extension of the microcracks are clearly larger in the spiral grooving surface patterns, whereas upon the knurling surface patterns these are minimized because the splats adapted better to the reduced geometry changes with effective deposition, then promoting the stacking and good inter-splat adhesion.
- Hard α - Al_2O_3 phase was consistently found throughout the coating in all specimens coming from both: a) the presence of partially melted and melted particles and, b) the formation of α - Al_2O_3 interlayers due to the multi-pass torch and the subsequent surface re-heating that produced reversed phase transformation from γ - Al_2O_3 to α - Al_2O_3 phase.
- The improved sliding wear resistance in the specimens with the knurling pattern was promoted

by the combination of γ - Al_2O_3 (toughness) and α - Al_2O_3 (hardness) phases through the thickness of the coating and, predominantly, by the reduced amount of porosity and microcracks that strengthen the inter-splat anchorage.

ACKNOWLEDGMENTS

Sara Isabel Zesati Belmontes want to thank the Mexican National Council on Science and Technology (Conacyt) for the financial support during this research project.

REFERENCES

- ASTM E384 (2017). Standard Test Method for Microindentation Hardness of Materials. ASTM International, West Conshohocken, USA.
- ASTM E2109-01 (2021). Standard Test Methods for Determining Area Percentage Porosity in Thermal Sprayed Coatings. ASTM International, West Conshohocken, USA.
- ASTM Committee (1994). *ASM Handbook "Surface Engineering"*. Vol 5, ASM International, Materials Park, OH, USA.
- Berndt, C.C., McPherson, R. (1979). The Adhesion of Flame and Plasma Sprayed Coatings - A Literature Review. *Australas. Weld. Res.* 6 (January), pp. 75–85.
- Bordeaux, F., Saint Jacques, R. G., Moreau, C. (1991). Study of surface preparation for enhanced resistance to thermal shocks of plasma-sprayed TiC coatings. *Surf. Coat. Technol.* 49 (1–3), 50–56. [https://doi.org/10.1016/0257-8972\(91\)90030-Z](https://doi.org/10.1016/0257-8972(91)90030-Z).
- Bordeaux, F., Jacques, R.G.S., Moreau, C., Dallaire, S., Lu, J. (1992). Thermal shock resistance of TiC coatings plasma sprayed onto macroroughened substrates. *Surf. Coat. Technol.* 53 (1), 49–56. [https://doi.org/10.1016/0257-8972\(92\)90102-G](https://doi.org/10.1016/0257-8972(92)90102-G).
- Davis, J.R. (2004). *Handbook Thermal Spray Technology*. ASM International, Materials Park, OH, USA.
- Di Girolamo, G., Brentari, A., Blasi, C., Serra, E. (2014). Microstructure and mechanical properties of plasma sprayed alumina-based coatings. *Ceram. Int.* 40 (8), 12861–12867. <https://doi.org/http://dx.doi.org/10.1016/j.ceramint.2014.04.143>.
- Fervel, V., Normand, B., Coddet, C. (1999). Tribological behavior of plasma sprayed Al_2O_3 -based cermet coatings. *Wear* 230 (1), 70–77. [https://doi.org/10.1016/S0043-1648\(99\)00096-4](https://doi.org/10.1016/S0043-1648(99)00096-4).
- Ghazali, M.J., Forghani, S.M., Hassanuddin, N., Muchtar, A., Daud, A.R. (2016). Comparative wear study of plasma sprayed TiO_2 and Al_2O_3 - TiO_2 on mild steels. *Tribol. Int.* 93, 681–686. <https://doi.org/10.1016/j.triboint.2015.05.001>.
- Habib, K.A., Saura, J.J., Ferrer, C., Damra, M.S., Giménez, E., Cabedo, L. (2006). Comparison of flame sprayed $\text{Al}_2\text{O}_3/\text{TiO}_2$ coatings: Their microstructure, mechanical properties and tribology behavior. *Surf. Coat. Technol.* 201 (3–4), 1436–1443. <https://doi.org/10.1016/j.surfcoat.2006.02.011>.
- Hollis, K.J., Bartram, B.D., Roedig, M., Youchison, D., Nygren, R. (2007). Plasma-sprayed beryllium on macro-roughened substrates for fusion reactor high heat flux applications. *J. Therm. Spray Tech.* 16 (1), 96–103. <https://doi.org/10.1007/s11666-006-9011-6>.
- Islak, S., Buytoz, S., Orhan, N., Stokes, J. (2012). Effect on microstructure of TiO_2 rate in Al_2O_3 - TiO_2 composite coating produced using plasma spray method. *Optoelectron. Adv. Mater. Rapid Commun.* 6 (9), 844–849.
- James, D.H. (1984). A review of Experimental Findings in surface preparation for thermal spraying. *J. Mech. Work. Technol.* 10 (2), 221–232. [https://doi.org/10.1016/0378-3804\(84\)90069-X](https://doi.org/10.1016/0378-3804(84)90069-X).
- Lou, H., Goberman, D., Shaw, L., Gell, M. (2003). Identification fracture behavior of plasma-sprayed nanostructured

- Al₂O₃-13wt.%TiO₂ coatings. *Mater. Sci. Eng. A* 346 (1–2), 237–245. [https://doi.org/10.1016/S0921-5093\(02\)00523-3](https://doi.org/10.1016/S0921-5093(02)00523-3).
- Matějčiček, J., Chráska, P., Linke, J. (2007). Thermal spray coatings for fusion applications - Review. *J. Therm. Spray Tech.* 16 (1), 64–83. <https://doi.org/10.1007/s11666-006-9007-2>.
- Matikainen, V., Niemi, K., Koivuluoto, H., Vuoristo, P. (2014). Abrasion, erosion and cavitation erosion wear properties of thermally sprayed alumina based coatings. *Coatings* 4 (1), 18–36. <https://doi.org/10.3390/coatings4010018>.
- McPherson, R. (1973). Formation of metastable phases in flame- and plasma-prepared alumina. *J. Mater. Sci.* 8, 851–858. <https://doi.org/10.1007/BF02397914>.
- McPherson, R. (1980). On the formation of thermally sprayed alumina coatings. *J. Mater. Sci.* 15, 3141–3149. <https://doi.org/10.1007/BF00550387>.
- Michalak, M., Sokołowski, P., Szala, M., Walczak, M., Łatka, L., Toma, F.-L., Björklund, S. (2021). Wear Behavior Analysis of Al₂O₃ Coatings Manufactured by APS and HVOF Spraying Processes Using Powder and Suspension Feedstocks. *Coatings* 11 (8), 879. <https://doi.org/10.3390/coatings11080879>.
- Normand, B., Fervel, V., Coddet, C., Nikitine, V. (2000). Tribological properties of plasma sprayed alumina-titania coatings: role and control of the microstructure. *Surf. Coat. Technol.* 123 (2-3), 278–287. [https://doi.org/10.1016/S0257-8972\(99\)00532-0](https://doi.org/10.1016/S0257-8972(99)00532-0).
- Oerlikon Metco (1945). *Metallizing Handbook*. Long Island City, N.Y.
- Paredes, R.S.C., Amico, S.C., d'Oliveira, A.S.C.M. (2006). The effect of roughness and pre-heating of the substrate on the morphology of aluminium coatings deposited by thermal spraying. *Surf. Coat. Technol.* 200 (9), 3049–3055. <https://doi.org/10.1016/j.surfcoat.2005.02.200>.
- Psyllaki, P.P., Jeandin, M., Pantelis, D.I. (2001). Microstructure and wear mechanisms of thermal-sprayed alumina coatings. *Mater. Lett.* 47 (1-2), 77–82. [https://doi.org/10.1016/S0167-577X\(00\)00215-9](https://doi.org/10.1016/S0167-577X(00)00215-9).
- Romero, R.R. (1990). *Machinery Repairman*. NAVEDTRA 12204-A. Naval Education and Training Program.
- Singh, V.P., Sil, A., Jayaganthan, R. (2011). A study on sliding and erosive wear behaviour of atmospheric plasma sprayed conventional and nanostructured alumina coatings. *Mater. Des.* 32 (2), 584–591. <https://doi.org/10.1016/j.matdes.2010.08.019>.
- Steffens, H.D., Babiak, Z., Gramlich, M. (1999). Some aspects of thick thermal barrier coating lifetime prolongation. *J. Therm. Spray Tech.* 8 (4), 517–522. <https://doi.org/10.1361/105996399770350197>.
- Tucker, R.C. (1974). Structure property relationships in deposits produced by plasma spray and detonation gun techniques. *J. Vac. Sci. Technol.* 11 (4), 725–734. <https://doi.org/10.1116/1.1312743>.
- Wang, Y., Jiang, S., Wang, M., Wang, S., Xiao, T.D., Strutt, P.R. (2000). Abrasive wear characteristics of plasma sprayed nanostructured alumina/titania coatings. *Wear* 237 (2), 176–185. [https://doi.org/10.1016/S0043-1648\(99\)00323-3](https://doi.org/10.1016/S0043-1648(99)00323-3).
- Wang, Y.Y., Li, C.J., Ohmori, A. (2005). Influence of substrate roughness on the bonding mechanisms of high velocity oxy-fuel sprayed coatings. *Thin Solid Films* 485 (1–2), 141–147. <https://doi.org/10.1016/j.tsf.2005.03.024>.
- Yang, Y., Wang, Y., Tian, W., Yan, D-ran, Zhang, J.-xin, Wang, L. (2015). Influence of composite powders' microstructure on the microstructure and properties of Al₂O₃-TiO₂ coatings fabricated by plasma spraying. *Mater. Des.* 65, 814–822. <https://doi.org/10.1016/j.matdes.2014.09.078>.
- Yilmaz, R., Kurt, A.O., Demir, A., Tatli, Z. (2007). Effects of TiO₂ on the mechanical properties of the Al₂O₃ - TiO₂ plasma sprayed coating. *J. Eur. Ceram. Soc.* 27, 1319–1323. <https://doi.org/10.1016/j.jeurceramsoc.2006.04.099>.
- Yilmaz, Ş. (2009). An evaluation of plasma-sprayed coatings based on Al₂O₃ and Al₂O₃-13 wt.% TiO₂ with bond coat on pure titanium substrate. *Ceramics International* 35 (5), 2017–2022. <https://doi.org/10.1016/j.ceramint.2008.11.017>.